

# Water productivity mapping using remote sensing data of various resolutions to support "more crop per drop"

Xueliang Cai,<sup>a</sup> Prasad S. Thenkabail,<sup>b</sup> Chandrashekhar M. Biradar,<sup>c</sup>  
Alexander Platonov,<sup>a</sup> Murali Gumma,<sup>a</sup> Venkateswarlu Dheeravath,<sup>d</sup>  
Yafit Cohen,<sup>e</sup> Naftali Goldshleger,<sup>f</sup> Eyal Ben-Dor,<sup>g</sup> Victor Alchanatis,<sup>e</sup>  
Jagath Vithanage,<sup>a</sup> and Anputhas Markandu,<sup>a</sup>

<sup>a</sup> International Water Management Institute, PO BOX 2075, Colombo, Sri Lanka  
x.cai@cgiar.org; a.platonov@cgiar.org; m.gumma@cgiar.org; j.vithanage@cgiar.org;  
m.anputhas@cgiar.org

<sup>b</sup> Southwest Geographic Science Center, U.S. Geological Survey (USGS), Flagstaff, Arizona  
86001, USA  
pthenkabail@usgs.gov

<sup>c</sup> University of Oklahoma, 101 David L. Boren Blvd, Norman, Oklahoma 73019, USA  
chandra.biradar@ou.edu

<sup>d</sup> United Nations Joint Logistic Center, Juba, South Sudan, Sudan  
Venkat.dheeravath@wfp.org

<sup>e</sup> Institute of Agricultural Engineering, Bet-Dagan 50250, Israel  
yafitush@volcani.agri.gov.il; victor@volcani.agri.gov.il

<sup>f</sup> Erosion Research Station, Ministry of Agriculture, Israel  
naftalig@moag.gov.il

<sup>g</sup> The Remote Sensing and GIS Laboratory, Tel-Aviv University, Tel-Aviv 69978, Israel  
bendor@post.tau.ac.il

**Abstract.** The overarching goal of this research was to map crop water productivity using satellite sensor data at various spectral, spatial, radiometric, and temporal resolutions involving: (a) Moderate Resolution Imaging Spectroradiometer (MODIS) 500m, (b) MODIS 250m, (c) Landsat enhanced thematic mapper plus (ETM+) 60m thermal, (d) Indian Remote Sensing Satellite (IRS) 23.5 m, and (e) Quickbird 2.44 m data. The spectro-biophysical models were developed using IRS and Quickbird satellite data for wet biomass, dry biomass, leaf area index, and grain yield for 5 crops: (a) cotton, (b) maize, (c) winter wheat, (d) rice, and (e) alfalfa in the Sry Darya basin, Central Asia. Crop-specific productivity maps were developed by applying the best spectro-biophysical models for the respective delineated crop types. Water use maps were produced using simplified surface energy balance (SSEB) model by multiplying evaporative fraction derived from Landsat ETM+ thermal data by potential ET. The water productivity (WP) maps were then derived by dividing the crop productivity maps by water use maps. The results of cotton crop, an overwhelmingly predominant crop in Central Asian Study area, showed that about 55% area had low WP of  $< 0.3 \text{ kg/m}^3$ , 34% had moderate WP of  $0.3\text{-}0.4 \text{ kg/m}^3$ , and only 11% area had high WP  $> 0.4 \text{ kg/m}^3$ . The trends were similar for other crops. These results indicated that there is highly significant scope to increase WP (to grow "more crop per drop") through better water and cropland management practices in the low WP areas, which will substantially enhance food security of the ballooning populations without having to increase: (a) cropland areas, and/or (b) irrigation water allocations.

**Keywords:** Crop water productivity, remote sensing, spectro-biophysical models, simplified surface energy balance model, MODIS, Landsat ETM+, IRS, Quickbird.

## 1 INTRODUCTION, BACKGROUND, AND RATIONALE

Water is one of the most critical resources for human life and survival. However, the stress on water use is only increasing with the global population expected to reach around 10 billion by 2050. Securing the food and livelihoods for the rapidly increasing populations will put heavy demand on water. Further, the populations in the emerging markets are becoming increasingly consumer oriented requiring more food and products which all require water to produce. On the other hand, climate change impacts are creating uncertainties in water availability due to changes in seasonal climate patterns, reduced glacier sizes, and heavy over-exploitation of ground water.

Reference 1 has shown that the possible biggest saving in water is likely to come from growing more food with less water (increasing water productivity (WP) or "more crop per drop" philosophy). Currently, there are tremendous differences in the quantum of water used to produce a unit of grain within and between farm fields in various parts of the world as a result of different water and farmland management techniques [2]. This opens up an opportunity to study the causes of differences in water use to produce unit of grain, pin-point areas where these differences occur, and strategize approaches of increasing water productivity.

Water productivity studies are generally conducted in four approaches: (a) field experiments, (b) soil-plant-atmosphere transfer and hydrological modeling, (c) coupling of hydrological models and remote sensing, and (d) remote sensing/GIS techniques alone. Numerous studies on WP have been conducted through field experiments. Zwart and Bastiaanssen [2] reviewed measured WP values ( $\text{kg}/\text{m}^3$ ) from 84 publications and indicated huge differences. Ref. 3, also based on literature review, further gathered WP values expressed in economic terms (United States dollars/ $\text{m}^3$ ) for 42 regions in 5 continents. The field experiments approach provides critical initial understanding of water productivity values. However, this method is time, labor, and money consuming [4]. Also, field experiment method is usually applicable only to small scale area and thus has enormous difficulties in addressing the issue of scale, which is a major concern in WP studies [5-7]. The second approach involves two types of modeling, soil-plant-atmosphere models such as Soil, Water, Atmosphere, and Plant (SWAP), and Decision Support System for Agrotechnology Transfer (DSSAT) focus on plant water cycling in soil, plant and atmosphere continuous processes, and estimates yield as a response to the processes. Distributed hydrological models such as Soil Water Assessment Tool (SWAT), and Options Analysis in Irrigation Systems (OASIS), have the potential to provide time series results across pre-set scales. However, modeling setup and calibration is again difficult in data scarce regions. Unavoidable assumptions impose uncertainties and errors to model outputs [8]. Some researchers tried to link hydrological models with remote sensing as the third approach. Land use/land cover information, crop biophysical parameters, yield and evapotranspiration interpreted from satellite images are taken as inputs to models [9] or as reference data for model calibration [10]. Remotely sensed spatial patterns can be well integrated with modeled time series ground processes, hence providing the greatest potential for improved understanding of WP variations and the causes. The fourth approach aims to employ remote sensing and Geographical Information Systems (GIS) to map WP across spatial and temporal scales. Ref. 11 firstly used remotely sensed data to estimate both crop yield and evapotranspiration for WP study in Bhakra command area, India. This approach was further developed to estimate both yield and actual evapotranspiration (ET) using Surface Energy Balance Model Algorithm for Land (SEBAL) [12]. Remote sensing approach overcomes data scarcity and scale limitations in conventional studies, reduces uncertainties, and covers large spatial domain over time. The inherent strength of remote sensing for WP mapping and nascent state of its development in terms of methods and approaches offer an opportunity to conduct systematic studies on agricultural water management performance evaluation.

Given the above background, the overarching goal of this paper was to develop methods and protocols of water productivity mapping (WPM) using remotely sensed data of various resolutions involving (a) Moderate Resolution Imaging Spectroradiometer (MODIS) 500m, (b) MODIS 250m, (c) Landsat enhanced thematic mapper plus (ETM+) 60m thermal, (d) Indian Remote Sensing Satellite (IRS) 23.5 m, and (e) Quickbird 2.44 m data.. The proposed approach involved mapping: (a) crop types, (b) crop productivity, (c) crop water use (or actual ET), and (d) water productivity. The Syr Darya river basin in the Central Asia was chosen as study area given the large and extensive irrigation in the areas developed during former Soviet Union Era. The study collected extensive dataset on biophysical, yield, meteorological, and land use gathered from the farm fields during the crop growing seasons of 2006 and 2007.

## 2 DEFINITION OF AGRICULTURAL WATER PRODUCTIVITY

Agricultural water productivity is the physical mass of production (e.g., biomass, grain yield) or economic value of production to quantum of water used or delivered for the production [13]. It measures how the system converts water into goods and services. The generic equation is:

$$WP \text{ (kg/m}^3 \text{ or } \$/\text{m}^3 \text{)} = \frac{\text{Output derived from water use (kg/m}^2 \text{ or } \$/\text{m}^2 \text{)}}{\text{Water input (m}^3/\text{m}^2 \text{)}} \quad (1)$$

Output derived from water use includes physical measures, e.g., crop yield, biomass, fish, and livestock production which are all expressed in unit of kilogram; it can be also expressed in economic values (e.g., dollars) like market value of grain yield and/or biomass. Water input can be gross inflow, net inflow, available water, irrigation, and actual evapotranspiration.

With the inherent strength of remote sensing, this study uses crop productivity expressed in kg/m<sup>2</sup> as numerator and crop consumptive water use (actual evapotranspiration) as denominator, both of which are derived from satellite data with ground information input.

## 3 STUDY AREA

Syr Darya river basin (SRB) is located in Central Asia, covering an area of 444,000 km<sup>2</sup> including parts of Kyrgyzstan, Tajikistan, Uzbekistan and Kazakhstan (Fig. 1). It receives snowmelt water from Himalayas and drains into Aral Sea. With diverse range of altitude from 0 to 7,500 meters above average sea level, the annual average temperatures range from -10 to 5 °C at higher elevations and up to 15 °C at lower reach. The crops grown in SRB are predominantly cotton along with maize, rice, alfalfa in summer season and wheat in winter. The annual diversion from SRB is almost equal to total annual inflow, which imposes serious problem for the eco-system of downstream area and the Aral Sea [14]. Excess irrigation also creates problems including sali-alkalization and water logging in the upper and middle reach.

Within SRB, two representative study areas (Galaba and Kuva; see Fig. 1), which are representative agricultural regions, were selected. Both sites are located in middle reach where irrigated areas are concentrated. The two sites have significant differences in soil fertility, crop and water management practices. Part of Galaba is strongly affected by soil salinity and has poor farming input, while Kuva is well cultivated and has higher production.

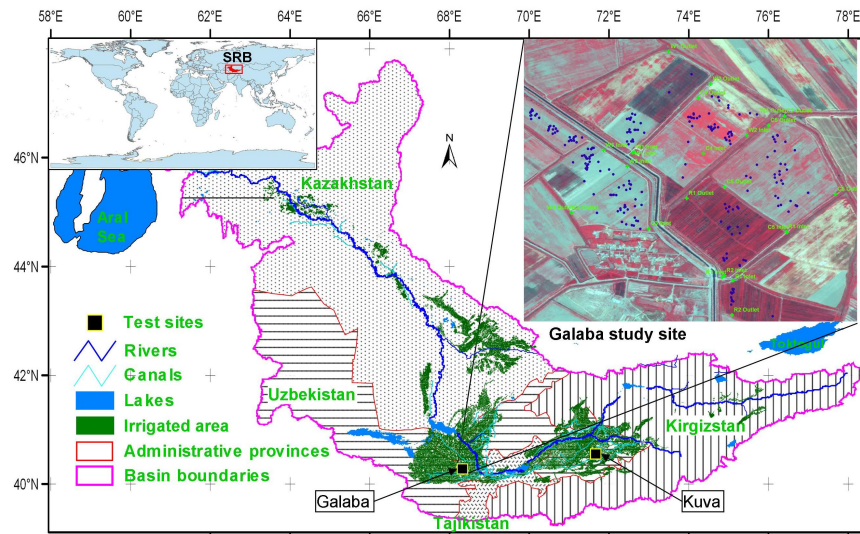


Fig. 1. Geographic location of the study area.

#### 4 DATA ACQUISITION AND CHARACTERISTICS

A wide array of data including satellite sensor imagery, routine collection of groundtruth data are gathered throughout the crop growing seasons of years 2006 and 2007 along with secondary GIS data including administrative boundaries, road, railway and river network, cities and agro-ecological zones.

##### 4.1 Satellite sensor data

Satellite sensor data at various resolutions were gathered for years 2006 and 2007. List of images are summarized in table 1.

Table 1. Satellite sensor data used in this study

Sensor	Resolution (m)	Image list
Quickbird	2.44	2006 Jul 26, Aug 3
IRS	23.5	2006: Apr 18, Jun 5, Jun 15, Jun 20, Jul 9, Jul 14, Jul 18, Aug 26, Sept 24, Oct 27, Nov 6; 2007: an 31, Apr 18, May 26, Jun 19, Jul 18, Aug 30, Sept 4
ETM+ thermal	60	2006 Apr 24, May 10, Jun 11, Jul 29, Aug 14, Oct 1
MODIS	250	Every 8 day for 2006
MODIS	500	Every 8 day for 2006

##### 4.2 Normalization of satellite sensor data

The Quickbird, IRS, and ETM+ sensors have different radiometric resolutions, spectral waveband widths [15-17], and the data are acquired in different days, time, view angles, and atmospheric conditions. Hence their respective digital numbers (DNs) carry different levels of information and cannot be directly compared. Therefore, they were converted to absolute units of radiance, then to at-sensor reflectance, and finally to surface reflectance after atmospheric correction.

While MODIS surface reflectance product data can be directly obtained from the United States Geological Survey (USGS) Earth Observing System Data Gateway (<http://edcimswww.cr.usgs.gov/pub/imswelcome/>). Data normalization of other sensors is more or less of similar steps. These include converting from DN to radiance using calibration factors as provided for in individual image header files. For Quickbird image this is:

$$L_{Pixel,Band} = absCalFactor_{\lambda} * DN_{i,j} \quad (2)$$

Where  $L_{Pixel,Band}$  is band integrated radiance ( $W m^{-2} sr^{-1}$ ),  $absCalFactor_{\lambda}$  ( $W m^{-2} sr^{-1} count^{-1}$ ) is absolute calibration factor as is 0.064 for Pan band, 0.016 for blue, 0.014 for green, 0.013 for red and 0.015 for NIR bands.  $DN_{i,j}$  is digital number (unitless) of pixel in row  $i$  and column  $j$ . Then the band average radiance can be calculated by dividing  $L_{Pixel,Band}$  by effective bandwidth.

IRS P6 spectral radiance ( $W m^{-2} sr^{-1} \mu m^{-1}$ ) was computed using the following equation:

$$L_{\lambda} = \frac{DN_{i,j} * Gain}{255} \quad (3)$$

The specific Gain ( $W m^{-2} sr^{-1} \mu m^{-1}$ ) settings of the bands are: for band 2 it is 26.609 for gain 1, 18.471 for gain 2, 12.064 for gain 3, and 8.988 for gain 4. Band 3 is 27.32, 18.179, 15.131, and 10.304 respectively. Band 4 is 31.018, 20.695, 15.757, and 10.876 respectively. For band 5 it can be further divided into two situations: where temperature  $<24^{\circ} C$  (6.903, 3.397, 1.644, 0.767) and  $\geq 24^{\circ} C$  (6.944, 3.406, 1.636, 0.752). These values could be obtained from the individual image header files.

The combined surface and atmospheric reflectance of the Earth is computed with the following formula [17]:

$$\rho_p = \frac{\pi * L_{\lambda} * d^2}{ESUN_{\lambda} * \cos(\theta_s)} \quad (4)$$

Where  $\rho_p$  is the at-satellite exo-atmospheric reflectance factor (unitless),  $d$  is the earth to sun astronomic distance (unitless) at the acquisition date,  $ESUN_{\lambda}$  ( $W m^{-2} sr^{-1} \mu m^{-1}$ ) is the mean solar exo-atmospheric irradiance, and  $\theta_s$  is solar zenith angle in degrees.

Time-invariant sites were used within image area to normalize multi-date imagery through use of perfect bright and perfect wet pixels as per the approach described in Ref. 18. In absence of perfect bright and wet pixels, atmospheric correction was performed using the improved dark object subtraction technique [19] to derive surface reflectance from at-sensor reflectance. All the images have been geo-referenced using Global Land Cover Facility (GLCF) Landsat ETM+ GeoCover products.

### 4.3 Field plot data

Field plot data was collected throughout the summer crop growing seasons (April-October) of 2006 and 2007 from the two study sites. Field visits were conducted around every 15 days and the data was collected for 5 crops: wheat, cotton, maize, rice and alfalfa. Measurements were carried out at randomly chosen points scattered in selected farms, resulting in 1003 records

from all the visits at different crop growing phases of 2006 and 2007. The items collected at each point include biophysical and yield variables of crops, land use/land cover measurements, soil variables, water variables, and metrological data (Table 2).

Cotton usually has more than one time harvests. Cotton yield in this paper is the sum of lint yield from first and second harvest. Visual estimations were made on field land cover (percentage crop canopy, water, weed, and soil). These data will be invaluable in crop type identification and in separating croplands versus non-croplands. An infiltration experiment was carried to determine soil water infiltration characteristics.

Table 2. Characteristics of field plot data used in this study.

Variable	Unit	Collecting Method	Sample size	Mean value	Sample size	Mean value	Sample size	Mean value	Sample size	Mean value
<b>A. General</b>			<b>Cotton</b>	<b>Cotton</b>	<b>Wheat</b>	<b>Wheat</b>	<b>Maize</b>	<b>Maize</b>	<b>Rice</b>	<b>Rice</b>
Coordinate	degree	Hand-held GPS	585	-	191	-	116	-	43	-
Soil type	-	Visual observation	15	-	15	-	6	-	2	-
<b>B. Crop variables for spectro-biophysical/Yield modeling</b>										
NDVI	-	NDVI camera	566	0.487	166	0.622	105	0.571	43	0.602
PAR	$\mu\text{mol m}^{-2}\text{s}^{-1}$	LAI meter	580	1060	174	1029	105	960.4	38	957.9
LAI	$\text{m}^2/\text{m}^2$	LAI meter	580	1.338	173	2.057	105	1.204	38	2.84
Wet biomass	$\text{kg}/\text{m}^2$	Cut and count	577	1.801	172	1.499	108	2.186	37	2.166
Dry biomass	$\text{kg}/\text{m}^2$	Cut and count	575	0.772	172	0.563	106	0.994	37	0.884
Crop height	mm	Ruler	576	453	172	569.5	108	920.9	41	610.2
Soil cover	%	Visual estimation	585	61.8	175	30.1	113	49.3	42	8.2
Canopy cover	%	Visual estimation	585	34.1	173	58.0	113	36.5	42	69.8
Yield	ton/ha	Laboratory	45	2.109	45	3.495	18	2.983	6	4.523
<b>C. Variables to study the factors affecting Water Productivity</b>										
EC	dS/m	EM-38 <sup>a</sup>	315	106.6	48	91.1	62	110.3	26	79.9
Soil moisture	%	Laboratory	36	12.55	9	16.9	15	11.95	6	18
Crop density	plant/ $\text{m}^2$	Cut and count	577	21.1	172	253.8	97	18.2	39	343.1
Weed cover	%	Visual estimation	585	5.0	173	12.9	108	14.4	42	10.6
Water cover	%	Visual estimation	585	3.51	173	0.56	108	0.01	42	13.7
Crop health	grading	Visual estimation	572	3.16	172	3.29	108	3.23	41	3.78
Crop vigor	grading	Visual estimation	573	3.00	172	3.09	108	3.03	41	3.61
<b>D. Meteorological variables for plant water use estimations or ET calculations</b>										
Air temperature	Celsius degree	Automated weather station <sup>b</sup>	5798	22.1						
Relative humidity	%		5798	50						
Wind direction	degree		5798	169.8						
Wind Speed	KM/h		5798	1.38						
Rainfall	mm		5798	151.8						
<b>E. Water applied measurements</b>										
Irrigation application	Mm	Weirs	5	293	2	80.57	4	158.9	4	355.2

Note: a = Average value of vertical and horizontal measurements were given.

b = the "watchdog" station was set up in Galaba site and the data was used for all crops.

## 5 METHODS

The methods for water productivity mapping using remote sensing are described in this section. Methods, broadly, consist of: (i) Crop productivity mapping; (ii) Water use mapping; and (iii) water productivity mapping.

### 5.1 Crop productivity mapping (kg/m<sup>2</sup>)

Crop productivity is the numerator of water productivity in this study. The crop productivity mapping has 3 distinct steps:

#### 5.1.1 Crop type mapping

Crop type map is essential to estimate crop yield and crop water consumption. With the rapid development of landuse/landcover (LULC) detecting techniques, the LULC dynamics including cropping patterns (e.g., crop area, crop type, and crop rotation) over larger area are made possible [20]. Mapping crop type dynamics requires multi-temporal image data covering different crop growing seasons, and involves sets of interpretation techniques. For example, harmonic analysis to identify crop types is widely adopted by using, e.g., AVHRR NDVI [21] and MODIS data [22]. Geerken et al. (2005) [23] developed conventional Fourier analysis and adopted a Fourier Filtered Cycle Similarity (FFCS) method. More studies used hierarchical crop mapping protocols involving a number of steps, e.g., decision tree [20, 24]. Rao developed crop specific spectral libraries first and then used them to distinguish crop types [25]. Further, Thenkabail et al proposed spectral matching techniques to group similar classes from time-series NDVI data and match them with ideal spectral data bank [26].

In this study, we used unsupervised classification backed by class identification and labeling protocols [26, 27] to develop crop type maps at various resolutions: MODIS 500m, MODIS 250m, IRS 23.5m, and Quickbird 2.44m. The process involved the use of spectral matching techniques to analyze the time-series images. The class identification and labeling process involved the use of bi-spectral brightness-wetness-greenness plots, space-time spiral-curves, Google Earth very high resolution imagery (for the areas outside Quickbird images), and groundtruth data [28]. A hierarchical class labeling system was adopted to synthesize subclasses. A groundtruth dataset containing GPS coordinates, pictures and visual observations carried out through the project period was used to support class identification and validation. The detailed procedure is beyond the scope of this paper but can be found in Ref. [27].

Winter wheat and cotton are the two major crops in SRB. However, the growing periods of these two crops are overlapping from April to June, meaning the two crops have to be grown in separate croplands. Wheat is almost the only crop in winter season, whereas there are other crops like rice, maize along with cotton in summer season. The growth period of common crops in SRB is shown in Table 3.

Table 3. Crop calendar of the five major crops in the Syr Darya river basin.

	Stage	Cotton	Winter wheat	Maize	Rice	Alfalfa
Growth Length (days)	Initial	30	30	20	25	
	Development	50	140	35	25	
	Middle	60	40	40	55	
	Late	55	30	30	25	
Dates	Sowing	15-Apr	10-Oct	10-Jun	21-May	2004-Sept
	Harvesting	15-Oct	10-Jun	10-Oct	28-Sep	2006-July

Note: the source is from combination of field survey and FAO irrigation and drainage paper 56 [29].

### 5.1.2 Spectro-biophysical/yield modeling

Quantitative relationships between spectral reflectivity versus grain yield and vegetation biophysical parameters help to monitor ecosystem and predict crop production. These models work in two distinct approaches: (a) physically based modeling and (b) statistical regression. Bastiaanssen and Ali (2003) [30] coupled photosynthetically active radiation (PAR) model [31], light use efficiency model [32], and surface energy balance algorithm for land (SEBAL) [33] into one model to estimate crop biomass and then yield employing harvest index (HI) concept. Some other models (e.g., Scattering by Arbitrary Inclined Leaves or SAIL) are widely used to produce crop parameters like leaf area index (LAI), which are then taken as inputs to crop growth models to predict potential yield [34]. Statistical regression is another popular way to model biophysical parameters [35]. Numerous models have been established using linear or non-linear equations based on data sourced from, e.g., AVHRR [36], MODIS [37], Landsat TM/ETM+ [35, 38, 39], ASTER [40], airborne [41], hyperspectral data [15, 42], and LIDAR [43]. While most of these models are accurate at farm plot level, their performance in consistent evaluation at regional scale over years is to be improved.

The NDVI, a combination of red and NIR bands to reflect vegetation healthiness, is extensively used in most of above mentioned studies. However, many studies also showed that involvement of other bands were equally important. Lee et al. (2004) [44] proved that NDVI, combined with surface temperature, soil moisture, and rainfall data can significantly improve crop yield estimation accuracy. Narrow bands from hyperspectral data showed strength in specific biophysical parameters modeling. It was found strong relationships with crop characteristics in specific narrow bands in the longer wavelength portion of the red (650-700 nm) [15, 42]. Similar findings were also observed for cotton crop in China [45]. Optimum use of spectral bands is essential in maximum utilization of remotely sensed data.

In this study, the spectral wavebands and two band vegetation indices (TBVIs) (independent variables) were related to biophysical variables and grain yield (dependent variables). The TBVIs consider all possible 2-band normalized indices [15, 42]. So, an IRS 4-band data have 6 unique 2-band indices which are: TBVI21, TBVI31, TBVI32, TBVI41, TBVI42, and TBVI43. For example, TBVI21 is defined as:

$$TBVI21 = \frac{Band2 - Band1}{Band2 + Band1} \quad (5)$$

Similarly, all unique indices from Quickbird are also considered for developing relationships with crop variables.

Spectral reflectance and TBVI values corresponding to groundtruth point locations were extracted from time series IRS images and related to field biophysical measurements made close to the image acquisition date. 25% of the points were reserved for validation. The well distributed IRS images improve the model input data coverage to most of crop growth period which makes the simulation more robust. However, Quickbird image is of one time hence is related to GT data of one date. Various types of spectro-biophysical/yield models including linear, multivariate linear, and non-linear (Quadratic, Logarithmic, Exponential, and Power) models were tested. The crop variables were modeled best based on the best fit  $R^2$  values. The multivariate linear models were established taking up to three variables as given in Eq. 6.

$$Y = a * x1 + b * x2 + c * x3 + d \quad (6)$$

Where Y is dependent variable (wet biomass, dry biomass, LAI and yield); x1, x2, x3 are independent variables (band spectral reflectivity and TBVIs); a, b, c and d are coefficients to be determined. The general trend observed is the more independent variables are taken, the

higher R-square values the model gets. For example, given model type of band spectral reflectance for wet biomass, the three-variable model has higher R-square value than two-variable model has. However, less variable model is preferred unless significant difference is in place ( $R^2$  difference > 0.1). Similar type of models were developed using data from other crops, other variables with spectral data from bands, and TBVIs for Quickbird instrument.

### 5.1.3 Extrapolation of models to larger spatial domains

The best spectro-biophysical/yield models were extrapolated to larger areas using crop type maps leading to crop productivity maps including variables such as biomass ( $\text{kg}/\text{m}^2$ ), LAI ( $\text{m}^2/\text{m}^2$ ), and yield (tonne/ha). Extrapolation of spectro-biophysical models to larger areas were possible only when models are robust and were developed based on extensive datasets, preferably, considering data from multiple dates and multiple seasons with spatially well distributed sample locations and having a large sample size [35] which were well satisfied in this study.

Spectro-biophysical models were established for individual crop. Hence they have to be applied to respective crop field only. Taking cotton as example, areas outside cotton fields were masked out from original IRS and Quickbird images using crop type maps. Biomass, LAI and yield models of cotton were setup in ERDAS Imagine "Model maker", and then applied to the image accordingly. In this way cotton productivity maps were produced.

## 5.2 Water use maps (actual evapotranspiration, mm)

Water used (actual evapotranspiration) by crops was determined based on Simplified Surface Energy Balance (SSEB) model [46] using thermal imagery and meteorological data. The SSEB assumes linear relationship between latent heat flux (ET) and land surface temperature. Hot pixel and cold pixel were used to represent "no ET" or "maximum ET" (potential evapotranspiration,  $ET_p$ ). Therefore, the actual ET ( $ET_a$ ) values of other pixels are linearly distributed between the range of hot pixel ( $ET_a=0$ ) and cold pixel ( $ET_a=ET_p$ ), resulting in a proportional ET fraction value ( $ET_{frac}$ ) for each pixel as expressed in Eq. 7:

$$ET_{frac} = \frac{T_H - T_x}{T_H - T_C} \quad (7)$$

Where,  $ET_{frac}$  is ET fraction ranging from 0 to 1,  $T_H$  and  $T_C$  are the temperature of hot and cold pixels respectively;  $T_x$  is the surface temperature of any pixel on the image. Actual ET of day  $i$  ( $ET_{a,i}$ ) map can be generated by multiplying  $ET_{frac}$  with  $ET_p$  of day  $i$  as shown in Eq. 8.

$$ET_{a,i} = ET_p * ET_{frac} \quad (8)$$

Ideally,  $ET_p$  should be spatially explicit as  $ET_{frac}$  does. However this was limited by the number of meteorological stations. In this study  $ET_p$  from single station was used.

### 5.2.1 $ET_{frac}$

Thermal bands of six Landsat ETM+ images acquired from April to October were used to derive  $ET_{frac}$  maps. Land surface temperatures were generated from the thermal bands for the sensor pass time and areas outside study extents were masked out.

Choosing of hot and cold pixels has to be carefully decided. Although some areas like concrete roads or settlements are likely to have higher temperature, hottest pixel should be

chosen from dry bare farm land where ET is almost zero while temperature is lower than the former. To avoid noise or effects of other extreme conditions, several (5-10) pixels, instead of single one, were chosen to calculate average values as for hot ( $T_H$ ) and cold ( $T_C$ ) pixel. The  $T_H$  and  $T_C$  were identified for each of the six land surface temperature maps. Using Eq. 7,  $ET_{frac}$  maps were generated.

### 5.2.2 Potential ET ( $ET_p$ )

Weather data from automated weather station is synthesized from hourly interval to daily basis and cross checked with weather data from nearby agro-climate station. These data were then used to calculate potential ET using Penman-Monteith equation and crop coefficients  $K_c$  as recommended by FAO.

### 5.2.3 Seasonal crop water use maps ( $ET_a$ ) (mm)

The seasonal crop ET ( $ET_{a,s}$ ) maps were produced by summing up the  $ET_a$  for the entire crop growth period. Ideally,  $ET_a$  is computed on a daily basis and summed up for the number of growing days. However, this is not feasible due to absence of daily high-resolution images. Three steps were involved to calculate  $ET_{a,s}$ .

(1)  **$ET_a$  maps of individual dates:**  $ET_a$  maps of the six individual dates corresponding to Landsat ETM+ images were produced by multiplying  $ET_p$  maps with  $ET_{frac}$  maps of the same dates using Eq. 8;

(2)  **$ET_a$  maps for crop growth period:** Crop growth period is identified in table 3. Monthly  $ET_a$  maps were produced first by multiplying  $ET_a$  of individual dates with 30 or 31 (number of days of the month). A partial period is used when the crop exists only in part of the month (e.g., if the crop is harvested on 12<sup>th</sup> of a month, then only 12 days of that month were used). The underlying assumption is that while  $ET_p$  varies,  $ET_{frac}$  remains constant throughout the entire month, which is a practical way to aggregate daily ET in a relatively short period (one month) in which no significant land cover changes occur. Sum of the monthly  $ET_a$  maps leads to evapotranspiration map for entire growth period.

(3)  **$ET_a$  maps for each crop:** Crop type maps were used to extract  $ET_a$  map for corresponding crop.

## 5.3 Water productivity maps ( $kg/m^3$ )

The output derived from water use in this study is wet/dry biomass and yield, which are all converted to the unit of  $kg/m^2$ . The crop water use as derived from remote sensing is actual ET in the unit of mm, which is converted to  $m^3/m^2$ . Water productivity maps were then produced by dividing the crop productivity maps by water use maps using Eq. 1.

## 6 RESULTS AND DISCUSSIONS

The results and discussions will first present crop productivity maps including crop type maps and biophysical models. This is followed by water use maps and then WP maps. The ability of satellite sensor data from MODIS 500m, MODIS 250m, IRS 23.5m, and Quickbird 4m in determining WP were examined and discussed.

### 6.1 Crop type maps

The irrigated areas for Galaba study site determined using satellite sensor data at various resolutions were summarized in Table 4. These areas were determined by considering sub-pixel areas of MODIS 250m and 500m maps [27] and full pixel areas of IRS and Quickbird. The results showed that the area of croplands (including farm fallows) increased with increase in spatial resolution of the imagery in the homogeneous contiguous irrigated areas of SRB.

This was because, in coarser resolution imagery, the fragmented areas such as road-network and wastelands often get added up to larger areas such as the irrigated areas. This will make the irrigated areas higher than they actually are. In contrast, in the finer resolution imagery these smaller fragmented classes separate themselves into distinct class of their own, which will lead to more precise estimate of irrigated areas.

Only IRS and Quickbird imagery were able to separate all the five crop types studied in this paper. Thereby, only IRS and Quickbird images were used further for WP estimates. The MODIS data had the ability to differentiate irrigated areas from other land use for dominate crops of cotton, wheat and to less accuracy, rice, but could not differentiate other crop types.

Table 4. Irrigated areas at 4 resolutions. The irrigated areas for Galaba study site as determined using satellite sensor data at 4 distinct resolutions. Unit: ha

<b>Aggregated Irrigated LULC type</b>	<b>Quickbird (2.4m)</b>	<b>IRS P6 (23.5m)</b>	<b>MODIS (250m)</b>	<b>MODIS (500m)</b>
Cotton	2068	4389	3897	5327
Wheat	N.A.	2068	3129	3197
Rice	318	363	444	0
Fallow	4033	1823	3029	3083

## 6.2 Spectro-biophysical models

The best spectro-biophysical/yield models were developed for each crop using the IRS and Quickbird data. The crop variables modeled were wet biomass (WBM, kg/m<sup>2</sup>), dry biomass (DBM, kg/m<sup>2</sup>), leaf area index (LAI, m<sup>2</sup>/m<sup>2</sup>), and grain yield (YLD, tonne/ha). Table 5 summarizes the best: (a) model type, (b) bands or indices involved, and (c) R<sup>2</sup>-values. Before analysis, 5% of the data points were sieved as outliers which could be caused by any minor mistakes in sampling, measuring and data recording. For the rest points, 75% were used in the modeling process and 25% were reserved for model validations. Unless mentioned in the footnote, all models were run using the pooled data of the Galaba and Kuva study areas for the years 2006 and 2007 except the ones reserved for validations.

An overwhelming proportion of the best models involved indices rather than wavebands (Table 5). The best models to determine WBM, DBM, LAI, and YLD were highly significant and explained around 80 percent variability using IRS data and about 70 percent variability using Quickbird data. The Quickbird models did not explain as much variability as IRS. This was because of the difficulty in the precise geo-location of the 2.44 m pixel. The uncertainty involved was slightly higher than IRS 23.5 m data. The best IRS-based models for cotton WBM (Fig. 2a), LAI (Fig. 2b), DBM (Fig. 2c), and YLD (Fig. 2d) are illustrated.

The frequency of occurrence of bands in the best models was determined to ascertain the importance of the bands from IRS and Quickbird data. The red (30%) and the near-infrared (28%) bands, which are required for computation of NDVI, were most frequently occurring. The green band (25%) follows closely. Blue band (11%) is not very critical in modeling crop variables. SWIR band (6%) was found, surprisingly, less important. There are few conventional NDVI based models provided high R-square values. For example, cotton wet biomass has an R-squared value of 0.83 involving IRS red band (band 2) and near-infrared band (band 3) (Table 5). However, there were several other models were non-conventional bands provided high r-squared values. For example, wheat wet biomass was modeled best with an R-squared value of 0.68 using IRS green band (band 1) and near infrared band (band 3) (Table 5). It is likely, that hyperspectral narrow-bands (not used in this study) can provide significantly higher R-squared values [42].

Table 5. Spectro-biophysical and yield models. The best models for determining biomass, LAI, and yield of 5 crops using IRS LISS and Quickbird data.

Crop	Parameter	Sensor	Best bands			Best indices			
			Sample size	Best model	Band	R-square	Best model	Band combination	R-square
<b>Cotton</b>	Wet Biomass	IRS	140	Exp	2	0.70	Power	2, 3	<b>0.83</b>
		QB	41	Multi-linear	1, 4	0.55	Power	3, 4	<b>0.68</b>
	Dry Biomass	IRS	136	Power	2	0.62	Power	2, 3	<b>0.82</b>
		QB	41	Exp	2	0.52	Exp	1, 2	<b>0.66</b>
	LAI	IRS	135	Multi-linear	3, 4	0.63	Power	1, 3	<b>0.73</b>
		QB	41	Multi-linear	2, 4	0.51	Exp	2, 4	<b>0.57</b>
	Yield	IRS <sup>A</sup>	14				Linear	2, 3	<b>0.70</b>
QB <sup>B</sup>		7				Linear	3, 4	<b>0.61</b>	
<b>Wheat</b>	Wet Biomass	IRS	9	Quadratic	2	0.43	Quadratic	1, 3	<b>0.68</b>
	Dry Biomass	IRS	14	Quadratic	1	0.21	Quadratic	3, 4	<b>0.31</b>
	LAI	IRS	18	Quadratic	4	<b>0.80</b>	Multi-linear	1,3; 2,3	0.47
	Yield	IRS	12				Linear	2, 3	<b>0.67</b>
<b>Maize</b> <sup>C</sup>	Wet Biomass	IRS	19	Power	2	0.82	Power	2, 3	<b>0.87</b>
	Dry Biomass	IRS	17	Exp	2	<b>0.93</b>	Power	2, 3	0.90
	LAI	IRS	19	Multi-linear	1, 3	0.78	Multi-linear	1,2; 2,3	<b>0.84</b>
<b>Rice</b> <sup>D</sup>	Wet Biomass	QB	10	Multi-linear	1, 2	0.54	Multi-linear	1,2; 2,4	<b>0.60</b>
	Dry Biomass	QB	10	Multi-linear	1, 2	0.40	Multi-linear	1,3; 2,3	<b>0.41</b>
	LAI	QB	10	Multi-linear	2, 4	<b>0.88</b>	Quadratic	2, 3	0.23
<b>Alfalfa</b>	Wet Biomass	IRS	21	Power	2	0.84	Quadratic	1, 2	<b>0.85</b>
		QB	8	Multi-linear	2, 4	0.77	Multi-linear	1,2; 2,3; 3,4	<b>0.89</b>
	Dry Biomass	IRS	21	Power	2	<b>0.82</b>	Exp	1, 2	0.81
		QB	8	Multi-linear	2, 4	0.73	Multi-linear	1,2; 2,3; 3,4	<b>0.87</b>
	LAI	IRS	21	Power	3	0.50	Exp	3, 4	<b>0.64</b>
		QB	8	Multi-linear	1, 3, 4	<b>0.93</b>	Multi-linear	1,3; 3,4	0.86

Note: A, Yield model using 2007 data  
 B, Yield model using 2006 data  
 C, Sample points from Quickbird for maize were inadequate  
 D, Sample points from IRS for rice were inadequate

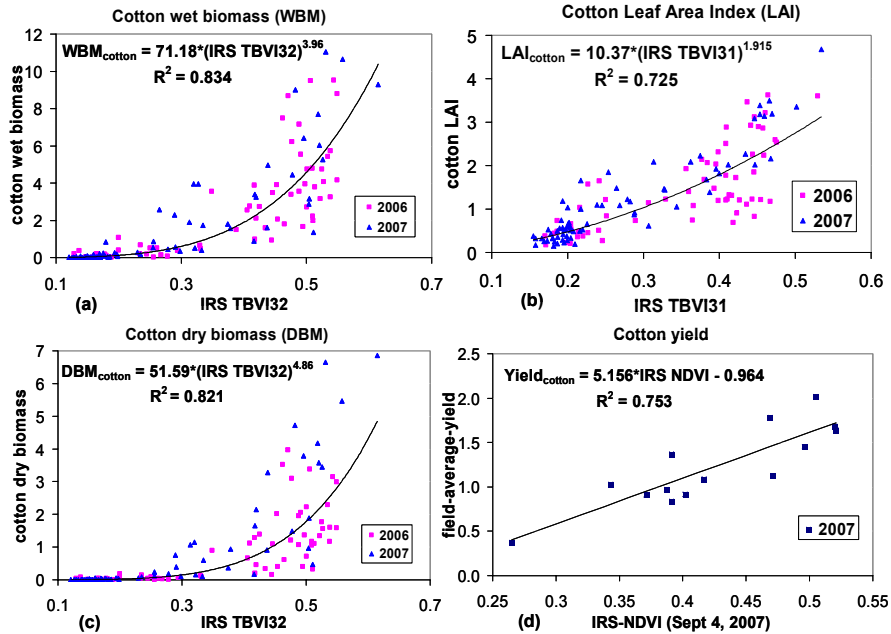


Fig. 2. The best spectro-biophysical models for cotton crop using IRS data. The models showing relationships of IRS derived indices with: (a) wet biomass, (b) LAI, (c) dry biomass, and (d) yield.

### 6.3 Crop productivity maps

The crop variable models developed using satellite sensor data at various resolutions were used to extrapolate the understanding to larger areas based on crop type map. In Fig. 3, crop productivity maps were determined for cotton biomass (Fig. 3a) and cotton yield (Fig. 3b) using the best IRS models on IRS imagery. These maps provide per pixel crop productivity in terms of biomass, yield and LAI.

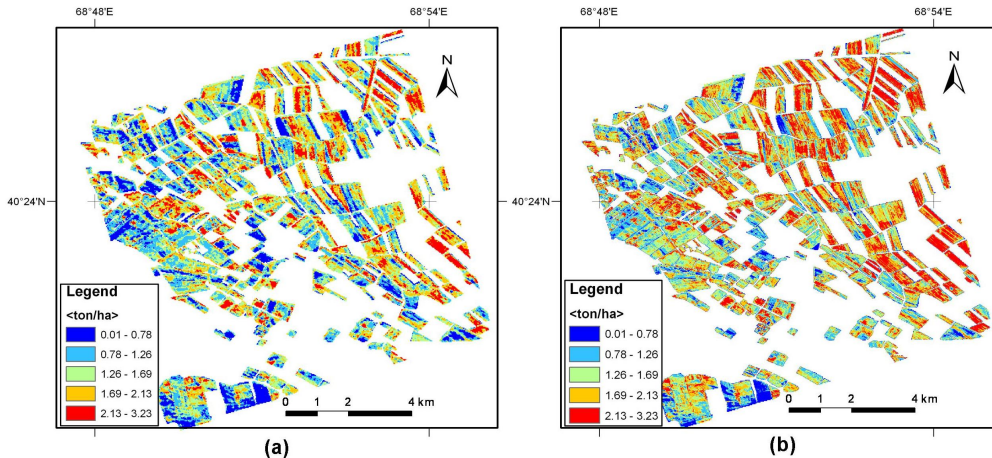


Fig. 3. Crop productivity maps for cotton in the Galaba study area using IRS data for: (a) wet biomass (18 Jul, 2006), and (b) yield (2006).

## 6.4 Water use (actual evapotranspiration) maps

ET<sub>a</sub> maps of the six individual dates were shown in Fig. 4. The six images, ranging from April to October, revealed significant spatial changes along cropping pattern changes. For example, a clear alternation of high ET in wheat and summer crop fields can be observed in the sequence of image date (from May 10 to June 11). Average seasonal water use for cotton was 512mm, ranging from 150 to 905 mm (Fig. 5a) and for rice 619mm, ranging from 165 to 769 mm (Fig. 5b). Although rice has much more short growing period than cotton, its daily water depletion is much higher, leading to higher total water use in its growing period. However, certain portions of cotton fields have much greater ET<sub>a,s</sub> (905 mm) than rice (769mm) which may be influenced by excellent growth conditions backed by longer growing period for cotton compared with rice.

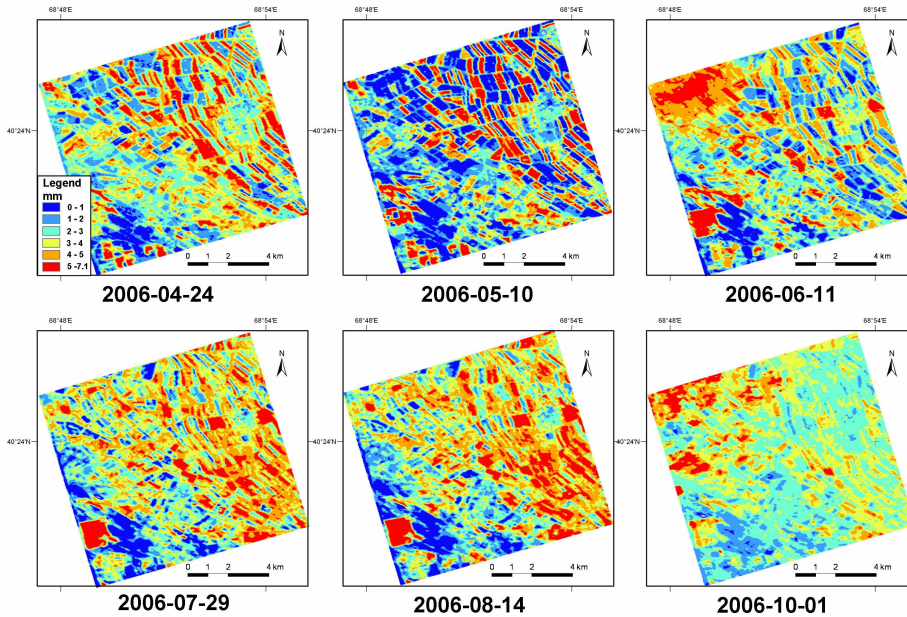


Fig. 4. Water use (ET<sub>a</sub>) maps for the Galaba study area derived from Landsat ETM+ and weather data.

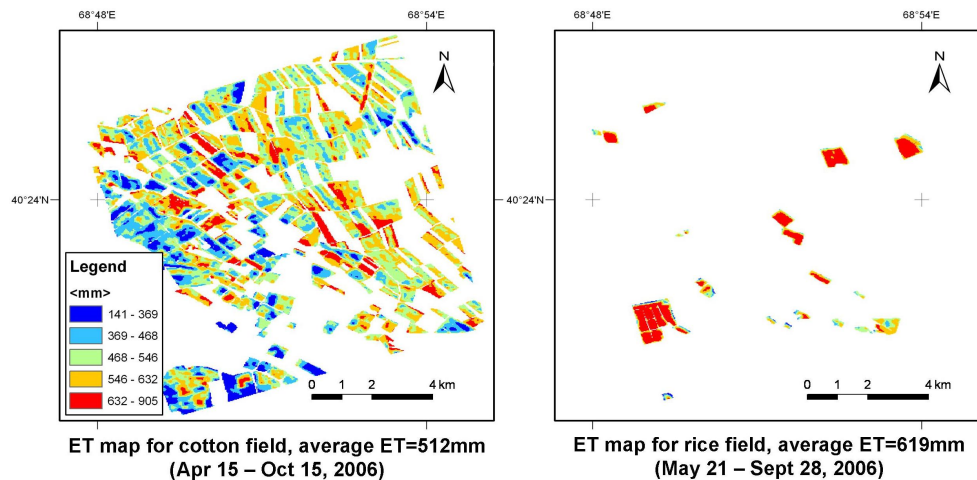


Fig. 5. Crop seasonal water use map in the Galaba study area for: (a) cotton crop and (b) rice crop.

The average  $ET_a$  of the study area from April 15 to October 15, 2006 is 502 mm. The  $ET_p$  of the same period is 1002 mm, almost double of the former, which can be explained by vegetation stress (e.g., water, salinity, nutrition, disease) experienced in the study area. Taking cotton as example, 1% of the cotton areas with an average yield of 2.5 tonne/ha, which is similar to field measured maximum yield, is considered as stress free areas with achievable yield. The average ET of the same area by SSEB is 861 mm. the potential ET calculated using FAO56 method, which in this case is actual ET, is 854 mm, which is very near to modeled values.

## 6.5 Water productivity maps

The water productivity maps have been produced for cotton, rice, wheat and maize using yield, wet and dry biomass as numerators in Eq. (9). Alfalfa is excluded in final WP maps because of its two-year growth period. Again taking cotton as example, the WP map for cotton yield using IRS and Quickbird were illustrated in figure 6. The average values of cotton WP were  $0.285 \text{ kg/m}^3$  from IRS data and  $0.289 \text{ kg/m}^3$  from Quickbird data. These values showed much higher variability ( $0-0.9 \text{ kg/m}^3$ ) compared with the reviewed range ( $0.1-0.35 \text{ kg/m}^3$ ) in Ref. 2 which were actually measured from limited number of field points, implying remote sensing approach picks up the extreme plots while field measurements tend to miss them. Both maps showed high similarities on how the WP distributes spatially, which indicates that it is possible to map WP variability using both IRS 23.5 m and Quickbird 2.44 m data. However, high resolution of Quickbird WP map explained more details compared to medium resolution of IRS map. Quickbird results generally have higher standard deviation, thus greater variability are captured. This enables to precisely pin-point areas that have lower or higher WP.

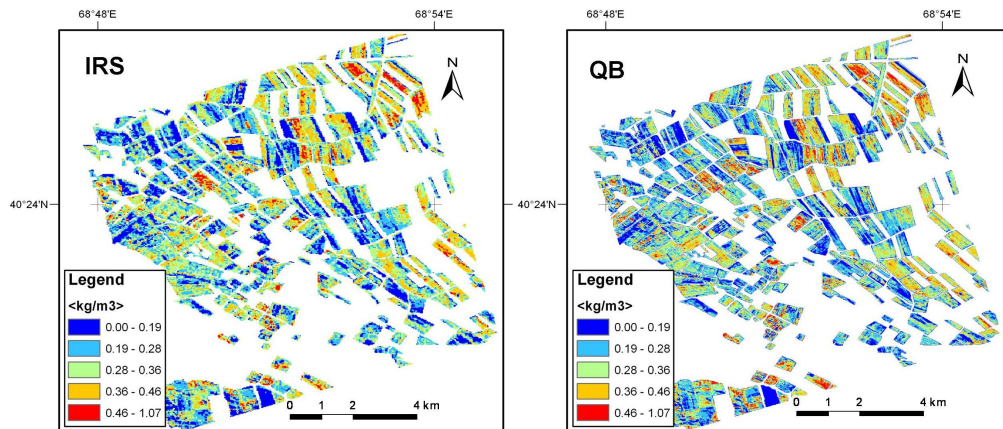


Fig. 6. Water productivity maps of cotton using: (a) IRS, and (b) Quickbird data.

The results in Table 6 show the areas under different water productivity groups. The WP of the irrigated cotton crop varied between  $0-0.9 \text{ kg/m}^3$ . Of this only 11 percent of the cotton crop area was in  $0.4 \text{ kg/m}^3$  or higher WP. About 55% of the cotton area had WP less than  $0.3 \text{ kg/m}^3$ . And 21% of area under very low WP ( $< 0.2 \text{ kg/m}^3$ ) based on IRS. This implies that there is highly significant scope to increase WP (to grow "more crop per drop") through better management practices. The challenge is to increase land and water productivity of the 55% low WP areas with a start on the 21% very low WP areas. The results had similar trends for other crops. Increasing the WP of these areas can greatly contribute to the food security of future generations without having to increase croplands and/or water use.

Table 6. Areas under different water productivity for cotton crop in Galaba determined using IRS and Quickbird data.

WP group (kg/m <sup>3</sup> )	IRS		Quickbird	
	area (ha)	share (%)	area (ha)	share (%)
0-0.1	167.9	4.1	85.1	1.8
0.1-0.2	695.5	16.8	970.2	21
0.2-0.3	1421	34.4	1550.7	33.5
0.3-0.4	1381.7	33.4	1370	29.6
0.4-0.5	414.7	10	542.7	11.7
0.5-0.6	50.3	1.2	93	2
>0.6	2.4	0.1	17.9	0.4

## 6.6 Model Validation

The validity of WP models produced in this paper were evaluated by first validating crop productivity (CP) models and then water use (actual ET) models.

The CP models were evaluated by using 25% of the total groundtruth data points that were reserved exclusively for model testing and validation. These reserved points were used to calculate model derived crop variables (taking best models reported in Table 5) and compared with the actual crop variables (from samples reserved for validation from Table 2). Generally, R-squares of modeled values versus actual values varied between 0.6 to 0.8 (e.g., illustrated for few variables in Fig. 7). The cotton crop yield models were highly correlated with actual yield with R-square values as high as 0.94 (Fig. 8).

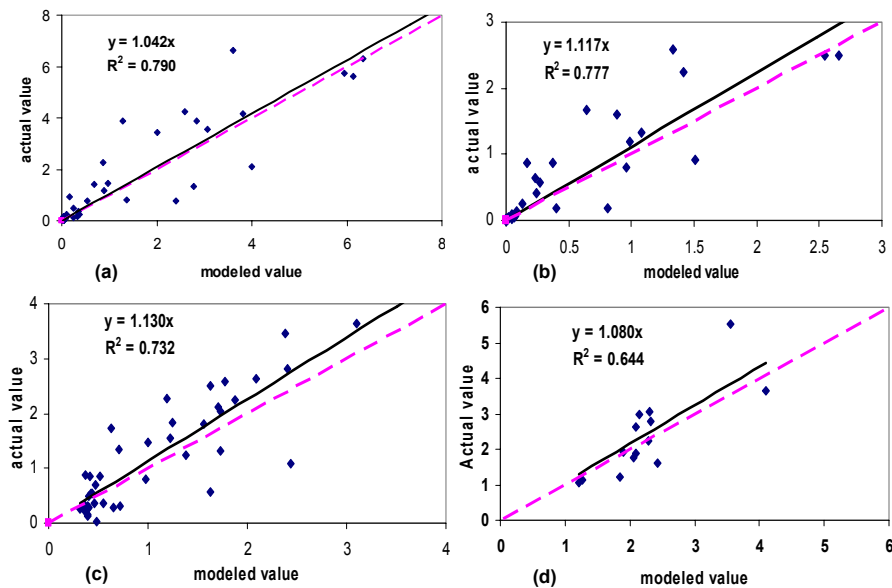


Fig. 7. Validation of best models. (a) Cotton wet biomass with IRS, (b) cotton dry biomass with IRS, (c) cotton LAI with IRS and (d) cotton LAI with Quickbird.

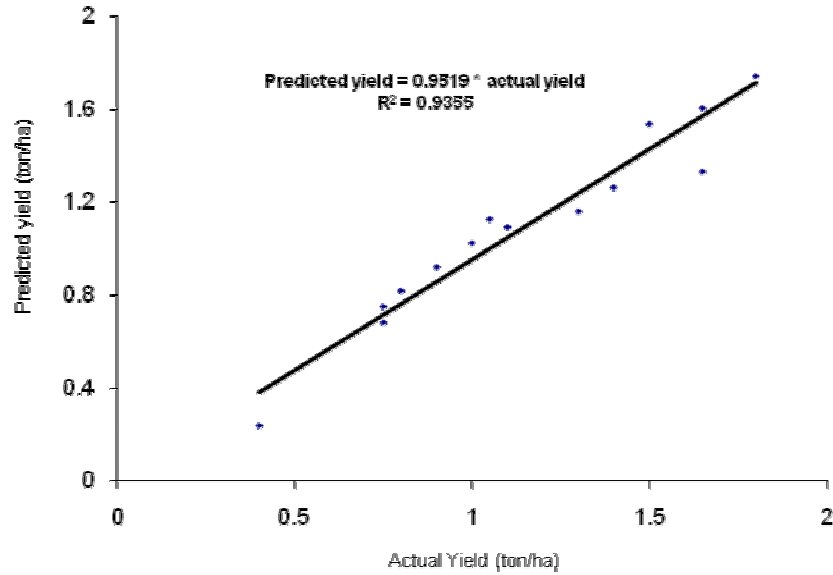


Fig. 8. Model validation for cotton crop yield.

Second part of the validation is to ensure water use (actual ET) is computed with accuracy. Actual ET models were built by multiplying evaporative fraction derived using Landsat thermal data with potential ET (see section 5.2). The potential ET is derived using well established Penman-Montieth equation [47] and crop coefficient ( $K_c$ ) approach as suggested by FAO [48]. Thereby, this leaves us with validation of ET fraction. For this we compared the SSEB derived ET fraction with that from METRIC and found high degree of assurance (R-square value of 0.77; see Fig. 9). The result clearly shows the reliability of SSEB as a simple yet efficient approach for ET fraction estimation.

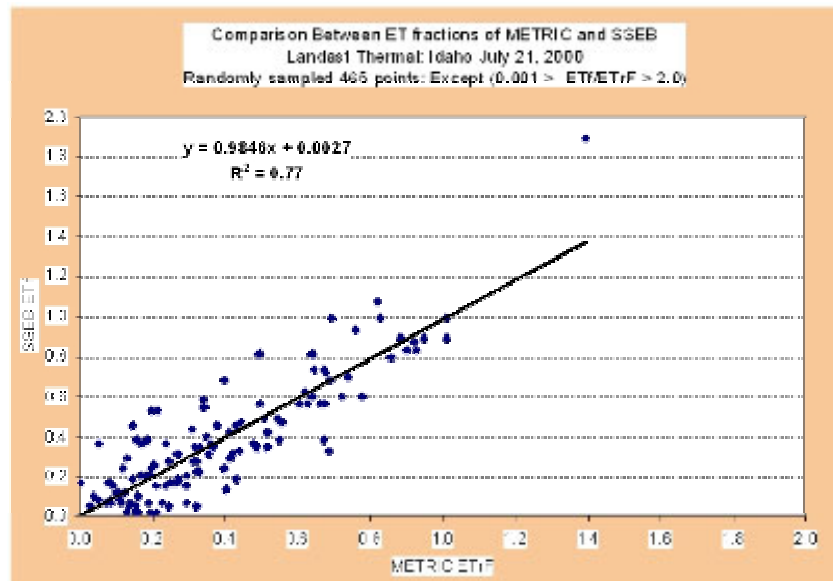


Fig. 9. Comparison between ET fraction from METRIC and SSEB models (personal correspondence with Dr. Gabriel Senay, developer of SSEB and Dr. Rick Allen, developer of METRIC).

## 7 CONCLUSIONS

This paper developed and illustrated methods and protocols for producing water productivity maps based on a study of five irrigated crop types (cotton, wheat, maize, rice, and alfalfa) and four crop variables (wet biomass, dry biomass, leaf area index, and grain yield) using remote sensing data at various resolutions. The methods involved: (a) crop type mapping, (b) spectro-biophysical modeling, (c) crop productivity maps by extrapolating the best spectro-biophysical models onto crop type maps, and (d) water use maps (or actual evapotranspiration) from ETM+ thermal data and point reference evapotranspiration, and (e) water productivity maps by dividing crop productivity maps by water use maps.

The best IRS and Quickbird spectro-biophysical models, mostly involving NIR and red bands, explained 65-90 percent variability in various crop variables. The IRS data explained about 10% greater variability than Quickbird. This was because of the uncertainty involved in precise location of a 2.44 m resolution Quickbird pixel.

The research demonstrated the ability to determine water used ( $ET_a$ ) by various crops during a growing season using remote sensing. Rice and cotton used maximum water of the 5 crops studied. Average seasonal water use of rice was 619 mm compared to 512 mm by cotton. However, certain portions of the cotton field that are in best growing conditions consumed more water (905 mm) than the highest consumed by rice (769 mm). This was also because of the significantly longer growing season for cotton (about 6 months) to rice (about 4 months). However, the percentage area of cotton consuming more water than rice was very limited. But, the results indicated that at best growing conditions, cotton can consume more water than rice due to its substantially longer growing period.

WP maps of the study area mapped using IRS data showed 55% of the total cotton area in low WP ( $<0.3 \text{ kg/m}^3$ ) of which 21% was in very low WP ( $<0.2 \text{ kg/m}^3$ ), 34% in moderate WP ( $>0.3 \text{ kg/m}^3$  but  $<0.4 \text{ kg/m}^3$ ), and only 11% of the total cotton area having high WP ( $>0.4 \text{ kg/m}^3$ ). The trends were similar for other crops. The Quickbird images provided similar trends in both study areas and hence further re-enforce the reported trends in WP variability using IRS. These results clearly imply the highly significant opportunities that exist for growing "more crop per drop" (increased WP) using the existing cropland and water resources to re-enforce food security in coming decades for ballooning populations.

Water productivity of crops reveals the crop outputs over given water input. It can be increased in 3 distinct approaches: increasing crop productivity (numerator), reducing water input (denominator), and combination of the two. In the study area of SRB in Central Asia, WP generally showed lower values compared to the other parts of the world (from literature), which means opportunity exists to increase significant proportion of WP. The water use (actual ET) is highly uneven while high ET is not necessarily linked to high yield or high WP. Better water management practices are required to reduce unnecessary ET, for example, evaporation from saline areas. Water productivity variations were attributed to many factors, as determined through farmer interviews: soil salinity (43%), water logging (31%), field leveling (13%), water deficit (7%) and some other factors such as weeds, soil moisture, and crop density 6%.

This paper showed the inherent strength of remote sensing in WP studies. While the maps help to identify the spatial variability of WP within and between fields, time series data will further ensure robust models to reveal the temporal variability. Also factors affecting WP could be further advanced by direct application of multi-temporal data, which brings significant added value to the WP maps leading to appropriate interventions to better manage land and water resources and enhance WP.

## References

- [1] S. Khan, R. Tariq, Y. Cui, and J. Blackwell, "Can irrigation be sustainable?" *Agric. Water Manage.* **80**(1-3), 87-99 (2006) [doi:10.1016/j.agwat.2005.07.006].
- [2] S. J. Zwart and W.G.M. Bastiaanssen, "Review of measured crop water productivity values for irrigated wheat, rice, cotton and maize," *Agric. Water Manage.* **69**, 115-133 (2004) [doi:10.1016/j.agwat.2004.04.007].
- [3] I. Hussain, H. Turrall, D. Molden, and M. D. Ahmad, "Measuring and enhancing the value of agricultural water in irrigated river basins," *Irrig. Sci.* **25**(3), 263-282 (2007) [doi:10.1007/s00271-007-0061-4].
- [4] M. D. Ahmad, T. Biggs, H. Turrall, and C. A. Scott, "Application of SEBAL approach and MODIS time-series to map vegetation water use patterns in the data scarce Krishna river basin of India," *J. Water Sci. Technol.* **53**(10), 83-90 (2006) [doi:10.2166/wst.2006.301].
- [5] D. Molden, H. M. Rust, R. Sakthivadivel, and I. Makin, "A water-productivity framework for understanding and action," In *Water Productivity in Agriculture: Limits and Opportunities for Improvement*, pp. 289-300, J. W. Kijne, R. Barker, D. Molden, Eds., CABI Publishing, Wallingford, CT(2003).
- [6] J. G. Wesseling and R. A. Feddes, "Assessing crop water productivity from field to regional scale," *Agric. Water Manage.* **86**(1-2), 30-39 (2006) [doi:10.1016/j.agwat.2006.06.011].
- [7] M. D. Ahmad, M. Giordano, H. Turrall, I. Masih, and Z. Masood, "At what scale does water saving really save water?" *J. Soil Water Conservat.* **62**(2), 29A-35A (2007).
- [8] K. Beven and A. Binley, "The future of distributed models: model calibration and uncertainty prediction," *Hydrolog. Process.* **6**(3), 279-298, (2006) [doi:10.1002/hyp.3360060305].
- [9] P. Droogers and W. G. M. Bastiaanssen, "Irrigation performance using hydrological and remote sensing," *J. Irrig. Drain. Eng.* **128**(1), 11-18 (2002) [doi: 10.1061/(ASCE)0733-9437(2002)128:1(11)].
- [10] W. W. Immerzeel, A. Gaur, and S. J. Zwart, "Integrating remote sensing and a process-based hydrological model to evaluate water use and productivity in a south Indian catchment," *Agric. Water Manage.* **95**(1), 11-24 (2008) [doi:10.1016/j.agwat.2007.08.006].
- [11] W. G. M. Bastiaanssen, S. Thiruvengadachari, R. Sakthivadivel, and D. Molden, "Satellite remote sensing for estimating productivities of land and water," *Int. J. Water Resour. Dev.* **15**(1/2), 181-196 (1999) [doi: 10.1080/07900629949005].
- [12] S. J. Zwart and W. G. M. Bastiaanssen, "SEBAL for detecting spatial variation of water productivity and scope for improvement in eight irrigated wheat systems," *Agric. Water Manage.* **89**(3), 287-296 (2007) [doi: 10.1016/j.agwat.2007.02.002].
- [13] D. Molden, "Accounting for water use and productivity," *SWIM Paper 1*, International Water Management Institute, Colombo, Sri Lanka (1997).
- [14] M. H. Rust, I. Abdullaev, M.H. Hassan, and V. Horinkova, "Water productivity in the Syr-Darya River basin," *IWMI Research Report 67*, Colombo, Sri Lanka (2003).
- [15] P. S. Thenkabail, E. A. Enclona, M. S. Ashton, C. Legg, and M. Dieu, "Hyperion, IKONOS, ALI, and ETM+ sensors in the study of African rainforests," *Rem. Sens. Environ.* **90**(1), 23-43 (2004) [doi:10.1016/j.rse.2003.11.018].
- [16] A. Melesse, Q. Weng, P. Thenkabail, and G. Senay, "Remote sensing sensors and applications in environmental resources mapping and modeling," *Sensors* **7**, 3209-3241 (2007) [doi: 10.3390/s7123209].

- [17] B. L. Markham and J.L. Barker, "Radiometric properties of U.S. processed Landsat MSS data," *Rem. Sens. Environ.* **22**, 39-71 (1987) [doi: doi:10.1016/0034-4257(87)90027-7].
- [18] C. D. Elvidge and Z. Chen, "Comparison of broad-band and narrow-band red and near-infrared vegetation indices," *Rem. Sens. Environ.* **54**(1), 38-48 (1995) [doi: 10.1016/0034-4257(95)00132-K].
- [19] P. S. Chavez, "Image-based atmospheric corrections - Revisited and Improved," *Photogramm. Eng. Rem. Sens.* **62**(9), 1025-1036 (1996)
- [20] B. D. Wardlow and S. L. Egbert, "Large-area crop mapping using time-series MODIS 250 m NDVI data: an assessment for the U.S. Central Great Plains," *Rem. Sens. Environ.* **112**(3), 1096-1116 (2008) [doi: 10.1016/j.rse.2007.07.019].
- [21] M. E. Jakubauskas, D. R. Legates, and J.H. Kastens, "Harmonic analysis of time-series AVHRR NDVI data," *Photogramm. Eng. Rem.Sens.* **67**(4), 461-470 (2001).
- [22] T. Sakamoto, M. Yokozawa, H. Toritani, M. Shibayama, N. Ishitsuka, and H. Ohno, "A crop phenology detection method using time-series MODIS data," *Rem. Sens. Environ.* **96**(3-4), 366-374 (2005) [doi: 10.1016/j.rse.2005.03.008].
- [23] R. Geerken, B. Zaitchik, and J. P. Evans, "Classifying rangeland vegetation type and coverage from NDVI time series using Fourier Filtered Cycle Similarity," *Int. J. Rem. Sens.* **26** (24), 5535-5554 (2005) [doi: 10.1080/01431160500300297].
- [24] M. Turker and M. Arikan, "Sequential masking classification of multi-temporal Landsat7 ETM+ images for field-based crop mapping in Karacabey, Turkey," *Int. J. Rem. Sens.* **26**(17), 3813-3830 (2005) [doi: 10.1080/01431160500166391].
- [25] N. R. Rao, "Development of a crop-specific spectral library and discrimination of various agricultural crop varieties using hyperspectral imagery," *Int. J. Rem. Sens.* **29** (1), 131-144(2008) [doi: 10.1080/01431160701241779].
- [26] P. S. Thenkabail, P. Rao, T. Biggs, M. Krishna, and H. Turrall, "Spectral matching techniques to determine historical land use/land cover (LULC) and irrigated areas using time series AVHRR Pathfinder Datasets in the Krishna River basin, India," *Photogramm. Eng. Rem. Sens.* **73**(9), 1029-1040 (2007).
- [27] P. S. Thenkabail, C. M. Biradar, P. Noojipady, V. Dheeravath, Y. J. Li, M. Velpuri, M. Gumma, G. P. O. Reddy, H. Turrall, X. L. Cai, J. Vithanage, M. Schull, and R. Dutta, "Global irrigated area map (GIAM) for the end of the last millennium derived from remote sensing," *Int. J. Rem. Sens.* (in press) (2009)
- [28] P. S. Thenkabail, M. Schull, and H. Turrall, "Ganges and Indus River basin land use/land cover (LULC) and irrigated area mapping using continuous streams of MODIS data," *Rem. Sens. Environ.* **95**(3), 317-341 (2005) [doi: 10.1016/j.rse.2004.12.018].
- [29] R. G. Allen, L. S. Pereira, D. Raes, and M. Smith, "Crop evapotranspiration: Guidelines for computing crop water requirements," *Irrigation Drainage Paper 56*, UN-FAO, Rome, Italy (1998).
- [30] W. G. M. Bastiaanssen and S. Ali, "A new crop forecasting model based on satellite measurements applied across the Indus basin, Pakistan," *Agric. Ecosyst. Environ.* **94**, 321-340 (2003) [doi: 10.1016/S0167-8809(02)00034-8].
- [31] J. L. Monteith, "Solar radiation and productivity in tropical ecosystems," *J. Appl. Ecol.* **9**, 747-766 (1972).
- [32] C. B. Field, J. T. Randerson, and C. M. Malmstrom, "Global net primary production: combining ecology and remote sensing," *Rem. Sens. Environ.* **51**(1), 74-88 (1995) [doi: 10.1016/0034-4257(94)00066-V].
- [33] W. G. M. Bastiaanssen, M. Menenti, R. A. Feddes, and A. A. M. Holtslag, "A remote sensing surface energy balance algorithm for land (SEBAL), 1. Formulation," *J. Hydrol.* **212-213**, 198-212 (1998) [doi: 10.1016/S0022-1694(98)00253-4].

- [34] P. C. Doraiswamy, J. L. Hatfield, T. J. Jackson, B. Akhmedov, J. Prueger, and A. Stem, "Crop condition and yield simulations using Landsat and MODIS," *Rem. Sens. Environ.* **92**(4), 548-559 (2004) [doi: 10.1016/j.rse.2004.05.017].
- [35] P. S. Thenkabail, "Biophysical and yield information for precision farming from near-real-time and historical Landsat TM images," *Int. J. Rem. Sens.* **24**(14), 2879-2904 (2003) [doi:10.1080/01431160710155974].
- [36] N. R. Dalezios, C. Domenikiotis, A. Loukas, S.T. Tzortzios, and C. Kalaitzidis, "Cotton yield estimation based on NOAA/AVHRR produced NDVI," *Phys. Chem. Earth* **26**(3), 247-251 (2001) [doi: 10.1016/S1464-1909(00)00247-1].
- [37] W. B. Cohen, T. K. Maersperger, Z. Y. Yang, S. T. Gower, D. P. Turner, W. D. Ritts, M. Berterretche, and S. W. Running, "Comparisons of land cover and LAI estimates derived from ETM+ and MODIS for four sites in North America: a quality assessment of 2000/2001 provisional MODIS products," *Rem. Sens. Environ.* **88**(3), 233-255 (2003) [doi: 10.1016/j.rse.2003.06.006].
- [38] D. Turner, W. Cohen, R. Kennedy, K. Fassnacht, and J. Briggs, "Relationships between leaf area index and Landsat TM spectral vegetation indices across three temperate zone sites - steps toward validating global map products," *Rem. Sens. Environ.* **70** (1), 52- 68 (1999) [doi: 10.1016/S0034-4257(99)00057-7].
- [39] D. Zheng, J. Rademacher, J. Chen, T. Crow, M. Bresee, J. L. Moine, and S. R. Ryu, "Estimating aboveground biomass using Landsat 7 ETM+ data across a managed landscape in northern Wisconsin, USA," *Rem. Sens. Environ.* **93**(3), 402-411 (2004) [doi: 10.1016/j.rse.2004.08.008].
- [40] N. J. Baptiste and J. R. Jensen, "Measurement of mangrove biophysical characteristics in the Bocozelle ecosystem in Haiti using ASTER multispectral data," *Geocarto Int.* **21**(4),3-8 (2006) [doi: 10.1080/10106040608542397].
- [41] P. K. Goel, S. O. Prasher, J.-A. Landry, R. M. Patel, A. A. Viau, and J. R. Miller, "Estimation of crop biophysical parameters through airborne and field hyperspectral remote sensing," *Trans. ASAE* **46**(4), 1235-1246 (2003).
- [42] P. S. Thenkabail, R. B. Smith, and E. De-Pauw, "Hyperspectral vegetation indices and their relationships with agricultural crop characteristics," *Rem. Sens. Environ.* **71**(2), 158-182 (2000) [doi: 10.1016/S0034-4257(99)00067-X].
- [43] L. Jennifer, R. Jensen, K. S. Humes, T. Conner, C. J. Williams, and J. DeGroot, "Estimation of biophysical characteristics for highly variable mixed-conifer stands using small-footprint LIDAR," *Can. J. Forest. Res.* **36**, 1129-1138 (2006) [doi: 10.1139/X06-007].
- [44] K. S. Lee, W. B. Cohen, E. Robert, R. E. Kennedy, T. K. Maersperger, and S. T. Gower, "Hyperspectral versus multispectral data for estimating leaf area index in four different biomes," *Rem. Sens. Environ.* **91**(3-4), 508-520(2004). [doi:10.1016/j.rse.2004.04.010].
- [45] H. Bai, K. Li, K. R. Wang, X. Y. Sui, and B. Chen, "Estimation models of cotton aboveground fresh biomass based on field hyperspectral remote sensing," *Agric. Sci. China* **33**(2), 311-316 (2007) [doi:10.1016/S1671-2927(07)60067-4].
- [46] G. B. Senay, M. Budde, J. P. Verdin, and A. M. Melesse, "A coupled remote sensing and simplified surface energy balance approach to estimate actual evapotranspiration from irrigated fields," *Sensors* **7**, 979-1000 (2007) [doi:10.3390/s7060979].
- [47] ASCE – EWRI. "The ASCE standardized reference evapotranspiration equation," ASCE-EWRI Standardization of Reference Evapotranspiration Task Comm. Report, (2005).
- [48] A. Kassam, and M. Smith, "FAO methodologies on crop water use and crop water productivity," *Expert Meeting Crop Water Productivity, Paper CWP-M07*, Rome, Italy (2001).

**Xueliang Cai** is a postdoctoral fellow at International Water Management Institute (IWMI), Colombo, Sri Lanka. Holding a PhD degree in irrigation engineering, he is well experienced in agro-hydrological modeling in irrigated agriculture. He also has the ability to apply remote sensing/GIS in agricultural land and water management research with various satellite sensor data (AVHRR, SPOT, MODIS, Landsat, IRS, ASTER, IKONOS, and Quickbird) for various applications, e.g., crop biophysical and yield modelling, ET mapping, LULC dynamic detection, and GIS based spatial modeling. He also possesses a large body of interdisciplinary research skills, e.g., statistical analysis (SAS), field irrigation experiments, socio-economic questionnaire survey and performance assessment. He has working experiences in China, Sri Lanka, Central Asia, India and South Africa.

**Prasad S. Thenkabail** is a research geographer at the U.S. Geological Survey, Flagstaff, Arizona, USA. An authority on global croplands using remote sensing, he recently published a book (as main editor) entitled: "Remote Sensing of Global Croplands for Food Security". Prior to this he was a principal researcher and head of remote sensing at the International Water Management (IWMI). Prasad has 23+ years experience working as a well recognized International expert in Remote Sensing and Geographic Information Systems (RS/GIS) and its applications to natural resources management, sustainable development, and environmental studies. He lead the global irrigated area mapping project and water productivity mapping project at IWMI. Prasad has worked in over 25 Countries in Africa, Asia, Middle-East, and North America. He has 60+ publications in major International journals. He is currently on the Landsat Science Team, editorial board of Remote Sensing of Environment (RSE), and one of the Associate Editor-in-Chiefs of Journal of Spatial Hydrology (JoSH).

**Chandrashekhar M. Biradar** is research scientist at Center for Spatial Analysis, University of Oklahoma, USA. Prior to this he was at the Institute for the Study of Earth, Oceans and Space, UNH. He is the author of more than 25 peer-reviewed scientific papers and book chapters and co-editor of two books. His current research interests include global land remote sensing; land use and land cover change, cropping intensity, climate change and ecology of infectious diseases.

**Alexander Platonov** is a National Researcher of the IWMI, Central Asia sub-office in Tashkent, Uzbekistan. He has 10 years experience as a GIS/RS specialist in projects for agricultural land and water resources management in Central Asian countries.

**Muralikrishna Gumma** is special project scientist at International Water Management Institute. He is the author of more than 20 peer-reviewed scientific papers and book chapters of two books. His current research interests include global land remote sensing; Identify the best sites in inland valleys wetlands rice cultivation in Africa, land use and land cover change, cropping intensity, climate change and ecology of infectious diseases. Murali recently completed his PhD.

**Venkateswrlu Dheeravath** currently works for the United Nations Joint Logistic Center (UNJLC), Juba, South Sudan as a GIS Manager. Earlier to this, Venkat was a regional research officer (remote sensing and GIS) at the International Water Management Institute (IWMI), Colombo, Sri Lanka. Venkat will soon defend his dissertation for a PhD. The topic of research was to map irrigated areas of India using MODIS data. He has Master's in Water Resources Engineering and Bachelor's in Civil Engineering.

**Yafit Cohen** is a researcher at the Institute of Agricultural Engineering, Agricultural Research Organization, Volcani Center, Tel Aviv, Israel. Her research interest includes Precision

agriculture: thermal and hyper-spectral imagery for monitoring and mapping water status and nitrogen level in various crops and orchards; Spatio-temporal analysis of pests and diseases: Medfly, Olive fly, Pear Psylla, and soil-borne diseases in potato and nuts; Development of spatial knowledge-based decision support systems for pest control; Remote sensing for recognition and mapping of crop types and delineation of Green corridors.

**Naftali Goldshleger** is a Researcher at the Institute of Agricultural Engineering, Agricultural Research Organization, Volcani Center, Tel Aviv, Israel.

**Eyal Ben-Dor** is a full professor at the Tel Aviv University (TAU) and was the chair of the Geography and Human Environment Department at Tel-Aviv University from 2005-2009. Currently he is serving as the head of the Remote Sensing Laboratory (RSL) within this department. He has more than 16 years experience in remote sensing of the Earth, with special emphasis on the Imaging Spectroscopy technology (IS) and soil spectroscopy. He has a strong background in soil science, spectroscopy, and remote sensing processing and is the author of more than 200 papers, book chapters and technical reports. Recently he was awarded by the Tel Aviv University President as an excellent research amongst the 1000 professors at the university and was appointed by the Ministry of Science to be the founder and leader of the Israeli Hyper spectral Group: Center of Excellence (IHSR-CE).

**Victor Alchanatis** is a Researcher at the Institute of Agricultural Engineering, Agricultural Research Organization, Volcani Center, Tel Aviv, Israel. His research interests are: Sensors for precision agriculture: hyperspectral and thermal imaging; Computer vision; Multispectral image processing; Quality Evaluation of agricultural products by non-destructive methods.

**Jagath Vithanage** is a national researcher at IWMI, Colombo, Sri Lanka.

**Anputhas Markandu** was a statistician at IWMI, Colombo, Sri Lanka. He is currently doing his PhD in Canada.